

Construction and Analysis of Simulated Venera and Magellan Images of Venus

R. E. ARVIDSON AND M. SCHULTE

*McDonnell Center for the Space Sciences, Department of Earth and Planetary Sciences,
Washington University, St. Louis, Missouri 63130*

AND

R. KWOK, J. CURLANDER, C. ELACHI, JOHN P. FORD, AND R. S. SAUNDERS

Jet Propulsion Laboratory, California Institute of Technology, Pasadena, California 91109

Received October 13, 1987; revised March 4, 1988

One-look Seasat radar images covering the Gran Desierto dune complex, Sonora, Mexico; the Appalachian Valley and Ridge Province; and accreted terranes in the central interior of Alaska were digitally processed to simulate both Venera 15, 16 images (1 to 3 km resolution) of Venus and image data expected from the Magellan mission (120 to 300 m resolution). Sinc filters were used to simulate the appropriate range and azimuth resolutions, speckle was introduced as multiplicative noise, and additive Gaussian noise was included to simulate expected signal to thermal noise ratios. The Gran Desierto dunes, the largest complex in North America, are not discernable in the Venera simulation, whereas the higher resolution Magellan simulation shows the dominant dune patterns and specular reflections from dune faces oriented perpendicular to the incident radar. Anticlinal and synclinal structures are evident in both simulations over the Appalachians, mainly because differential weathering and erosion left resistant units as topographic highs that delineate the folds. The Magellan simulation also shows that fluvial processes have dominated erosion and exposure of the folded structures. Mountainous terrains and their degree of erosion are discernable in both simulations over Alaska, although only the Magellan simulation shows that fluvial, glacial, and aeolian processes have all been active in shaping the landscape. Neither simulation provides evidence that diverse lithotectonic terranes in Alaska were juxtaposed (i.e., accreted), since the primary evidence needed is lithological, whereas radar returns are dominated by topography and surface roughness, parameters only weakly indicative of lithology. Venera data show clear evidence for volcanic and tectonic terrains on Venus, i.e., endogenic landforms (V. L. Barsukov *et al.* 1986, *Proc. Lunar Planet. Sci. Conf. XVII, Part 2, J. Geophys. Res.* 91, D378–D398). On the other hand, the simulations suggest that determination of the nature and extent of terrain modification by exogenic processes (e.g., atmosphere–surface weathering, erosion, deposition) on Venus will remain uncertain, since the length scales of features diagnostic of such processes may be too small to be discerned from Venera data. Substantial differential weathering, erosion, and deposition may have occurred on Venus, enhancing the appearance of both volcanic and tectonic features. Alternatively, rates of resurfacing by volcanic and tectonic processes may have been much higher than rates of atmosphere–surface interactions, producing a surface dominated by volcanic burial and tectonic disruption. The simulations suggest that Magellan data may provide the critical fine-scale morphological information needed to test between these two alternative resurfacing scenarios. © 1988 Academic Press, Inc.

1. INTRODUCTION

The geology of Venus is a topic of growing interest to the Earth and planetary sciences community, since Earth-based radar images (Campbell *et al.* 1983, 1984, Jurgens *et al.* 1980), combined with the Soviet Venera 15, 16 orbital images (Barsukov *et al.* 1986) (Table I) show an abundance of evidence for a relatively young surface with extensive faulting, folding, and volcanism (e.g., Basilevsky *et al.* 1986, Barsukov *et al.* 1986, Crumpler *et al.* 1986, Bindschadler and Head 1987). The extent to which such exogenic processes as mass wasting, corrosion of surface materials due to reactions with the atmosphere, and aeolian erosion and deposition have operated is less clear. One objective of this paper is to use simulated Venera images of various terrains on Earth to explore the extent to which evidence for landform modification by exogenic processes can be extracted from data with Venera image characteristics. A second objective is to repeat the exercise using simulated Magellan images

for the same terrains. Magellan is an Orbiter scheduled for launch in 1989 that includes a radar system that will acquire global imaging data with an order of magnitude better resolution than Venera (Table I). A third objective is to use results from the analysis of the simulations to help formulate scenarios for resurfacing of Venus that (a) are consistent with our current level of understanding of the nature of the Venusian surface and (b) can be refined and tested with Magellan data.

This paper is organized as follows. First, the simulation algorithm, based on one-look Seasat data, is discussed. Use of the algorithm to simulate both Venera and Magellan images is integrated into the discussion. Both Venera and Magellan simulations for the terrestrial targets are then evaluated for geological information content, stressing evidence for the nature and extent of landform modification by exogenic processes. Plausible Venusian resurfacing scenarios are then discussed, along with the use of Magellan data to refine and evaluate the proposed resurfacing models.

TABLE I
COMPARISON OF MAGELLAN AND VENERA MISSION PARAMETERS

	Venera 15/16	Magellan	Seasat
Operating altitude (km)	1000–2000	250–3500	800
Orbital period (hr)	24	3.2	1.5
Attitude control	Gas	Momentum wheels	
SAR antenna (m)	6 × 1.4 Parabolic	3.7 Dish	2.1 × 10.7 Planar array
Transmitter type	TWT	Solid state	Solid state
Peak power (W)	80	350	1000
Radar frequency (GHz)	3.75	2.38	1.28
Radar bandwidth (MHz)	0.65	2.26	19
Ground range resolution (m)	1000–2000	120–300	25
Azimuth resolution (m)	1000–3000	120	25
Looks	4–10	4–20	4
System signal-to-noise (dB)	Unknown	5	12
Coverage (%)	25	Global	Selective
Incidence angle (deg)	7–17	15–45	23
Swath width (km)	120	20–25	100
Polarization	HH	HH	HH

Notes. Incidence angle is defined as the angle that the incident radar beam makes relative to the local surface normal. Angles quoted are for level terrains. Incidence angles will be lowest at high northern latitudes for Magellan.

2. GENERATION OF DEGRADED RADAR IMAGES FROM SEASAT DATA

Several terrestrial targets were chosen for the radar simulations analyses in order to cover the major exogenic processes that operate on Earth (Fig. 1). The Gran Desierto in Sonora, Mexico, is the largest dune complex in North America and thus provides an example of landforms produced by aeolian processes. The Appalachian Valley and Ridge Province in Pennsylvania provides landforms related to compressional folding and faulting associated with formation of the Appalachians, together with substantial differential weathering and fluvial erosion. The area chosen in Alaska includes a variety of tectonic, erosional, and depositional landforms. In each case, one-look Seasat images provided the starting point for generating simulated Venera and Magellan images. Table I provides a summary of Seasat, Venera, and Magellan radar characteristics.

The key parameters to be simulated for synthetic aperture radar images are spatial resolution (both range and azimuth), num-

ber of looks, system signal-to-noise ratio (SNR), and incidence angle. Noise due to both speckle and to the system must be included. Speckle noise is multiplicative and is inversely proportional to the square root of the number of looks. System noise is assumed to be dominated by additive thermal noise that determines the system SNR, the expected ratio of signal power to system noise power. Ambiguities, saturation, bit error, and quantization noise are assumed to be small relative to the noise floor. All of these parameters must be accounted for in realistic ways.

Single-look Seasat image data were selected to generate the simulations because Seasat has similar incidence angles and better quality characteristics than either Venera or Magellan. For example, single-look Seasat images have a 7×6 -m slant range resolution, a SNR considerably better than Magellan and (presumably) Venera, and an incidence angle close to those for Venera and similar to the incidence angle expected for higher latitude Magellan data (Table I).

A flow diagram illustrating the steps in generating the simulations is shown in Fig. 2. During the first step, the spatial resolution of the Seasat images was degraded by convolving the image with the following point spread function, $h(x,y)$:

$$h(x,y) = \text{sinc} \left[\frac{\pi x}{\delta r} \right] \text{sinc} \left[\frac{\pi y}{\delta a} \right], \quad (1)$$

where

$$\text{sinc}(z) = \frac{\sin(z)}{z}, \quad (2)$$

x, y = output image spatial frequencies in m, n directions; and δr and δa are the range and azimuth resolutions, respectively.

This procedure is equivalent to low-pass filtering or band-limiting the image data in the spatial frequency domain. A cubic spline interpolator was then used to resample the images to the specified pixel spacing. The resampled images have large num-



FIG. 1. North America map with radar image simulation sites.

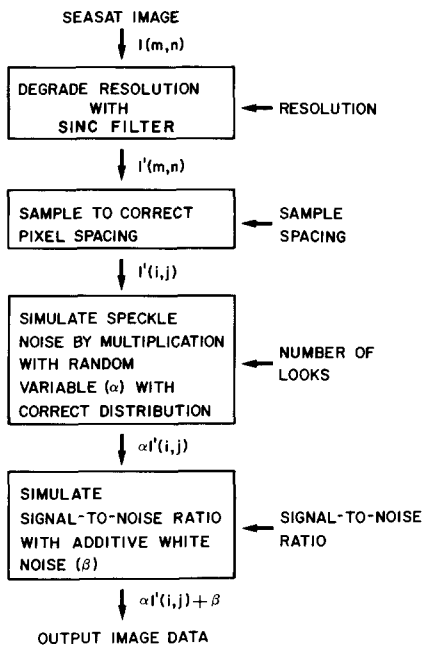


FIG. 2. Radar image simulation flow diagram.

bers of looks due to the low-pass filter applied during the first step. To simulate the correct number of looks, speckle noise was introduced as a multiplicative noise process (Goldfinger 1982), such that

$$I_s(i,j) = \alpha I'(i,j), \quad (3)$$

where

$$\alpha = \frac{1}{N} \sum_{i=1}^N \nu_i, \quad (4)$$

ν_i = Rayleigh distributed variate; N = number of looks; $I'(i,j)$ = input image value at line, sample, i,j ; $I_s(i,j)$ = output image value at i,j with speckle included. The speckle parameter α is governed by the multilook Rayleigh distribution and is the mean of N independent Rayleigh-distributed variates (ν_i). The speckle field is then correctly oversampled to reflect the oversampling of the image data.

Finally, the additive noise level is increased (from that of the Seasat data) to that expected in the simulated data by adding Gaussian white noise, β ,

$$I_0(i,j) = \alpha I'(i,j) + \beta, \quad (5)$$

where $I_0(i,j)$ = final output image.

The resulting images then have the correct resolution and are contaminated by the expected amount of multiplicative (speckle) and additive noise. Table II shows the parameters for each of the images used in the simulation process and the size of the output images. In each case the data are shown in a Universal Transverse Mercator projection (UTM). Note that the SNR of the simulated Venera images was not altered because the value of this parameter was not known to us. However, examination of the Venera images suggests the SNR is substantially lower than the values for Seasat. Thus, the Venera simulations provide best case images.

TABLE II
SIMULATED VENERA AND MAGELLAN IMAGE PARAMETERS

Scene	Venera 15/16 Pixel spacing: 750 m Signal-to-noise ratio: Unknown			Magellan Pixel spacing: 75 m Signal-to-noise ratio: 5 dB		
	Res (km)	Looks	Size (km)	Res (m)	Looks	Size (km)
Appalachian Valley	1.5 × 1.5	8	100 × 100	250 × 120	9	100 × 100
Gran Desierto	1.5 × 1.5	8	100 × 100	250 × 120	9	100 × 100
Alaska	1.5 × 1.5	9	440 × 300	250 × 120	16	440 × 300

Note. Resolution (Res): range × azimuth ground resolution. Size: width × height. Seasat images have approximately the same incidence angle: 23°. All images were written to film with a pixel size of 12.5 μ m.

The Alaska simulation is a mosaic assembled from 32 Seasat frames from five adjacent passes. The mosaic was generated using an automatic mosaicking system for generating digital mosaics from geocoded image frames (Kwok *et al.* 1988, in preparation). To produce a mosaic, each image frame was first put into UTM coordinates based on knowledge of the orbital geometry. Relative location errors between the adjacent image frames were measured by cross-correlation of selected image features at the overlapping regions. The images were then geometrically corrected to minimize these errors. The absolute location accuracy of the mosaic is approximately 60–100 m for the one-look data.

Radiometric disparities at the seams for the Alaska mosaic were cosmetically smoothed by a technique known as “feathering.” This technique is essentially the same as the one which will be used for the mosaicking of Magellan images. Feathering was done as follows: At the midpoint of the overlap region, the pixel values are set to the value M ,

$$M = \frac{M_1 + M_2}{2}, \quad (6)$$

where M_1 and M_2 are the means of images 1 and 2 at the overlap. The pixel values in the two images are then scaled with the function

$$S(k) = \begin{cases} \left[\frac{S_1 - 1}{N} \right] k + S_1, & k \leq 0, \\ - \left[\frac{S_2 - 1}{N} \right] k + S_2, & k \geq 0, \end{cases} \quad (7)$$

where $k = -N, \dots, 0, \dots, N$; $S_1 = M/M_1$; $S_2 = M/M_2$; and $2N$ is the number of pixels in the transition region. This region extends outside the overlap and is chosen such that there is a smooth transition of the pixel values from one image to the next. For the Alaska mosaic, the region extends

out to a hundred pixels ($N = 100$) from the center of the overlap region.

3. ANALYSIS OF SIMULATED VENUSIAN RADAR IMAGES

In this section, each of the simulated images will be evaluated for relevant geological information content. Recognition of evidence for exogenic processes will be stressed. Further, the extent to which diagnostic features can be recognized from radar data of any resolution will also be addressed. The last topic is especially relevant for Venus, where interpretations must be done in isolation of field or laboratory data, without much three-dimensional (i.e., structural) control, and using a system (i.e., active microwave) that is not directly sensitive to lithological variations. The Alaska scene will be emphasized because it covers an area comparable to the typical regions that are analyzed for Venera data (e.g., Barsurkov *et al.* 1986) and because it is the site of on-going studies by one of us (J.P.F.).

3.1. Gran Desierto, Sonora, Mexico

Figure 3 is a Landsat thematic mapper band 4 image of the Gran Desierto dune complex in Sonora, Mexico. The image, with 30-m-wide picture elements, clearly shows the extensive accumulation of dunes. In fact, transport directions can be inferred. On the right-hand side of the image, coalescing barchanoid dunes (D-3 to E-5) imply transport from the Gulf of California northward toward the Pinacate volcanic field (E-1 to E-4), a shield-like accumulation of flows and pyroclastic deposits. To the west, the largest dune structures in the complex are elongated in a NW–SE direction (B-3 to C-4), with a ridge-to-ridge spacing of approximately a kilometer. Star dunes sit atop the ridge crests, with NE–SW elongations (Greeley *et al.* 1985). Sand streaks extend in NW–SE directions in the upper left (A-1), with coalescing barchanoids between the streaks and the main dune structures (B-2). Transport from

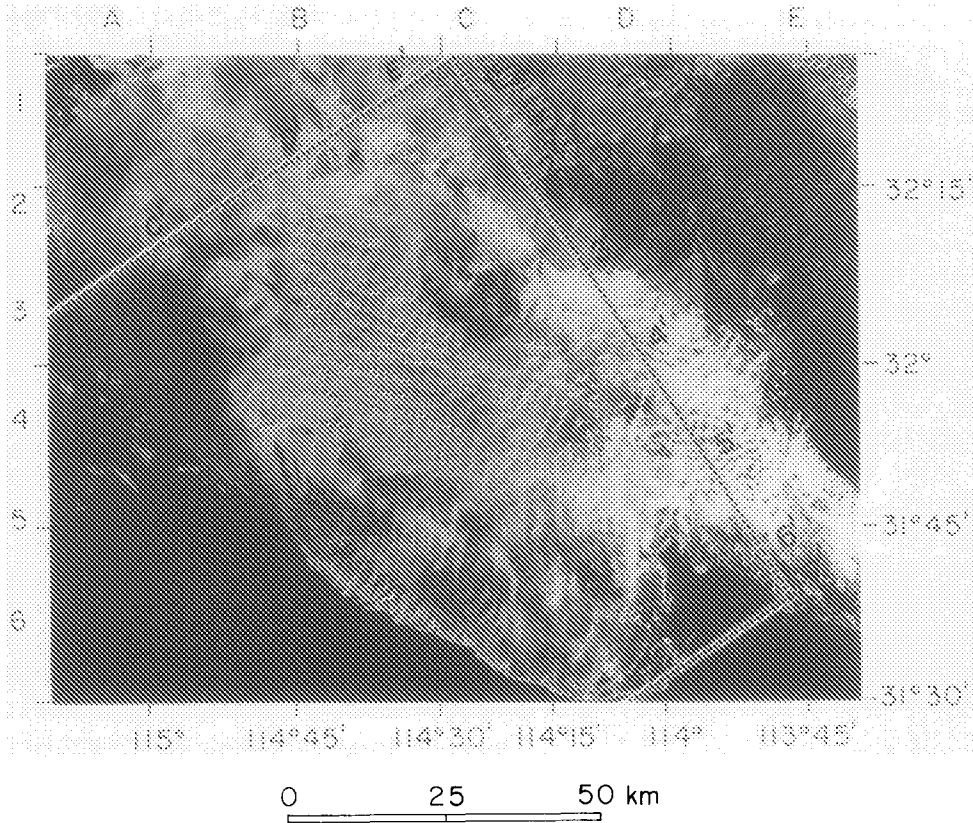


FIG. 3. Landsat thematic mapper band 4 image of Gran Desierto dune complex. Border shows approximate location of Venera and Magellan radar simulations shown in Fig. 4.

the NW to SE is implied, with the Colorado River valley (upper left) as the likely source of much of the sand. Finally, coalescing barchanoids at the southern edge (B-5 to C-5) of the main dune field also imply transport from the coast north toward the complex.

Figure 4 shows the Venera simulation of the dune complex. The Colorado River Valley and the Gulf of California dominate the left-hand edge of the scene (A'-1' to C'-6'). The main dune ridges appear as slightly brighter zones as does the barchanoid complex at the SW edge of the Pinacates (E'-5'). However, it is doubtful from this image alone that a reliable interpretation of dune fields would be made. Thus, the largest dune complex in North

America would probably go unnoticed if sampled with a system with characteristics similar to those for Venera.

The Magellan simulation, with an order of magnitude better resolution, provides direct evidence for the dune complex. The dominant NW-SE trending ridges are slightly brighter on the sides facing the radar (C'-2' to D'-3'). Further, a number of specular returns can be seen on the ridges, coming from the star dune faces that are oriented at right angles to the incident radar beam (e.g., Blom and Elachi 1981). The streaked patterns and the barchanoids can be delineated to the south of the main complex (E'-4' to E'-5'), and the mottled pattern to the south of the Pinacates is suggestive of dunes. Clearly, the order of

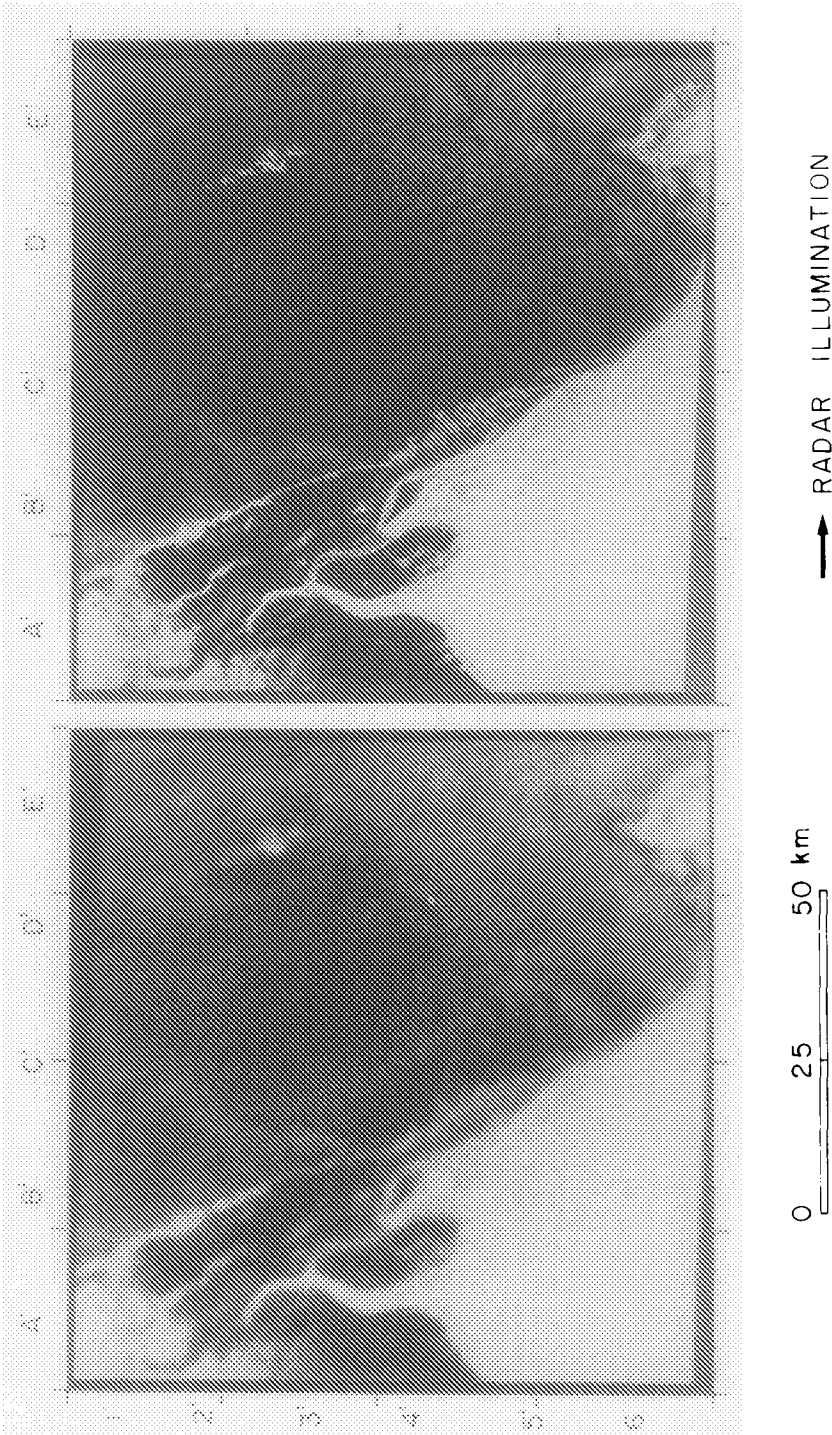


FIG. 4. Venera (left) and Magellan (right) radar image simulations of Gran Desierto region.

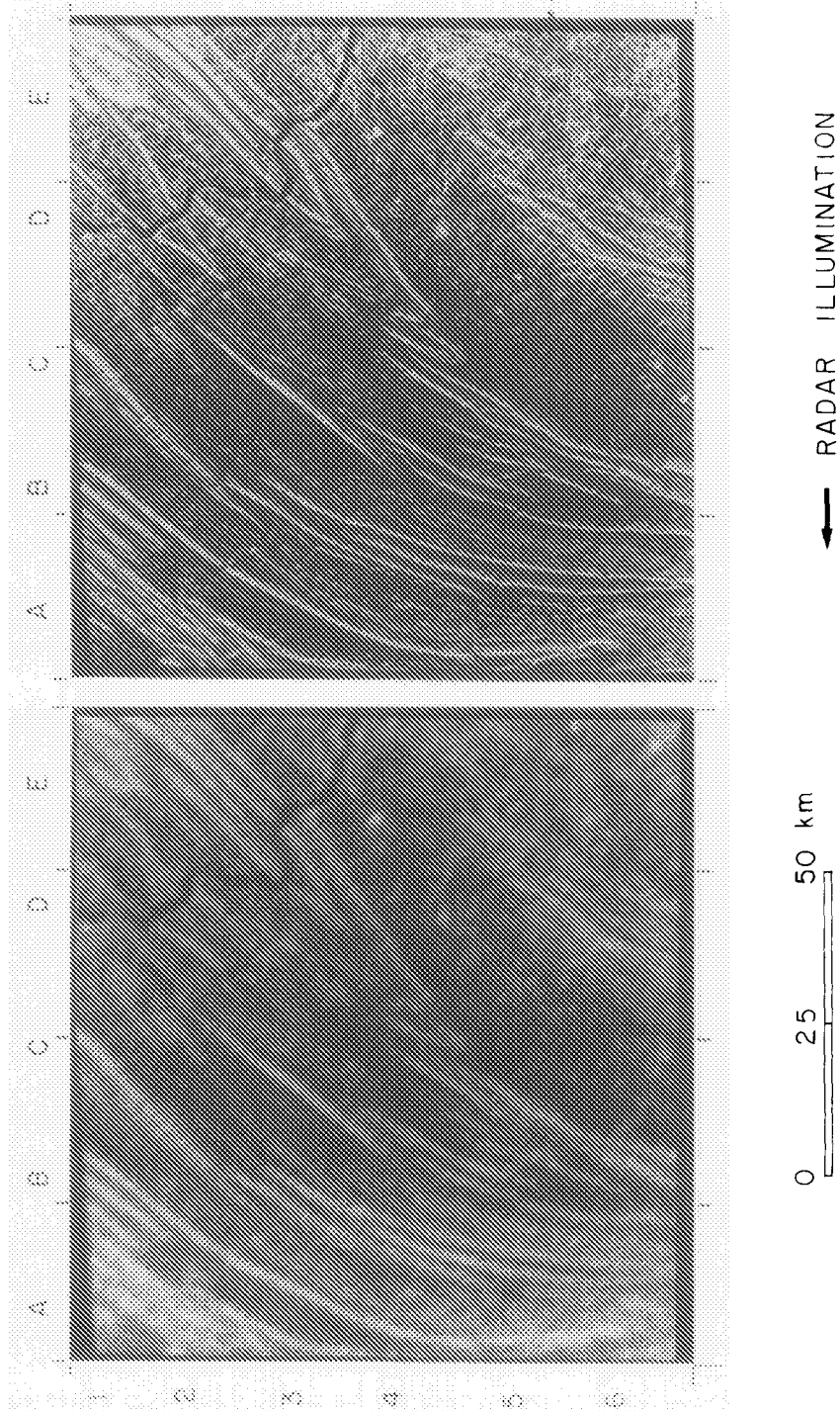


FIG. 5. Venera (left) and Magellan (right) radar image simulations of part of the Appalachian Valley and Ridge Province.

magnitude increase in resolution from Venera to Magellan is needed to identify and characterize the aeolian landforms in this case. On the other hand, based on previous studies (e.g., Blom and Elachi 1981), depending on the incidence angle and the orientation of the radar beam relative to the dune faces, the appearance of the field will vary dramatically, hampering complete inventory of the features with one radar image.

3.2. *Appalachian Valley and Ridge Province*

Figure 5 shows the Appalachian Valley and Ridge Province simulations, Fig. 6 is a

simplified geologic map, and Fig. 7 shows a cross-section of units along a traverse through the area covered by the Seasat data. Examination of the map and cross-section demonstrates that this area has been intensely folded and faulted. The compressional features are associated with formation of the Appalachian Mountains by convergence during the Paleozoic and Mesozoic Eras (Rodgers 1982). The map and section have resistant quartzites, sandstones, and conglomerates delineated. These rock types form topographic highs because they resist erosion as compared to the interbedded softer shales and limestones. In fact, although anticlinal and syn-

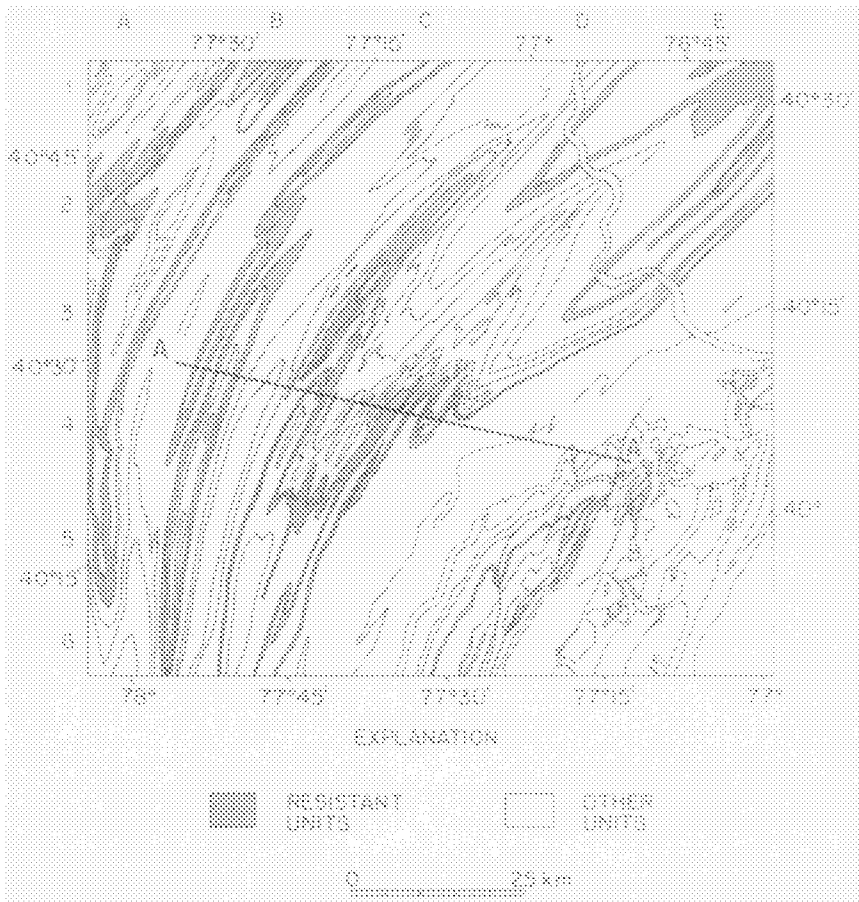


FIG. 6. Map showing outcrops in the Appalachian area. Data from Penn. Geol. Survey (1960). The stippled units are resistant rocks that include the Antietam Formation (quartzite and quartz schist), the Pocono Group (conglomerates, sandstones), the Pottsville Group (sandstones, conglomerates), and the Tuscarora and the Shawangunk Formations (quartzite, conglomerates). Cross-section A-A' shown in Fig. 7.

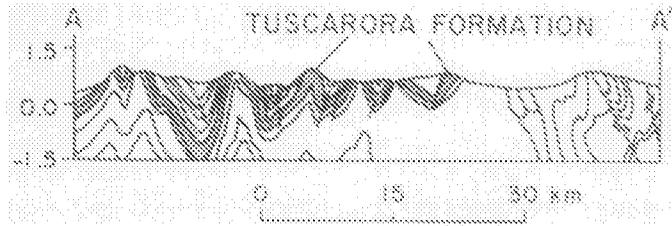


FIG. 7. Cross-section A-A' through the Appalachian area shown in Fig. 6. Vertical scale in kilometers.

clinal folding dominates the scene, surface expressions of these compressional structures are clear because of extensive differential weathering and subsequent fluvial erosion.

The Venera simulation of the Appalachian scene shows that radar returns are controlled by topographic highs plunging along broad anticlinal and synclinal structures. Bright foreslopes illuminated by the radar and dark backslopes offer convincing evidence that these returns are due to topography. The Magellan Valley and Ridge simulation, with an order of magnitude greater resolution, adds much fine-scale topographic information, including details of layering within the less resistant units. Most importantly, however, the Magellan simulation shows the dissected nature of the terrane, including water-gaps and other valleys cut into the resistant units. For example, the trellis dissection pattern on the backslope of the hill underlain by the Tuscarora Formation at location B-2 to A-5 is particularly diagnostic. Thus, the resolution characteristics of Magellan data allow recognition of structures, show the extent of weathering and erosion, and provide information concerning the surficial processes involved in enhancing the exposure of the structures by differential weathering and erosion.

3.3. Alaska Mosaic

Magellan and Venera simulations made from the Alaska mosaic are shown in Figs. 8A and 8B, respectively. The Alaska simu-

lation covers an area about 440×300 km in eastern interior Alaska, mostly located between latitudes 64–68 deg N and longitudes 144–153 deg W. This area contains dissected mountainous terrains that are interspersed with marginal upland and contiguous lowlands adjacent to the major streams. Figure 9 shows the generalized lithology of the area, and Fig. 10 is a cross-section.

The highlands are located in four distinct areas from north to south that include the southern foothills and the Philip Smith Mountains of the Brooks Range (Fig. 8, C-1 to D-1 to C-2 to D-2), the Kokrines Hills–Ray Mountains–Hodzana Highland (A-4 to C-2), the Yukon–Tanana Upland (B-4 to D-4 to C-5 to D-5), and the northern foothills and mountains of the Alaska Range (B-6 to C-5 to C-6). The highest peaks covered by the mosaic are approximately 2000 m in elevation in the Alaska and the Brooks Ranges. Steep slopes up to 30° and local relief up to 1000 m are common in the highland areas. The highlands are underlain by a wide range of complexly deformed, predominantly Precambrian through lower Paleozoic metasedimentary and metaigneous rocks (Beikman 1980, and sources quoted therein). Younger and less deformed continental sedimentary rocks are distributed on the northern foothills of the Alaska Range. Felsic plutons of Mesozoic age are widely distributed from the Ray Mountains through the Hodzana Highland to the Brooks Range. Late Paleozoic to Mesozoic mafic volcanic rocks extend

across large areas of the western Yukon–Tanana Upland and elsewhere in the highlands.

Because of their widely divergent lithotectonic origins and their juxtaposition along fault boundaries, the Paleozoic and early Mesozoic rock sequences in the highland areas, as in much of Alaska and elsewhere in western North America, have been interpreted to represent slabs of crust that were added to the preexisting continent by piecemeal accretion during late Mesozoic

and Cenozoic time (Coney *et al.* 1980, Churkin *et al.* 1982, Jones *et al.* 1981, 1984). The crustal slabs are referred to as accreted terranes, and are evident in the cross-section shown in Fig. 10. Most of the terrane boundaries are known or suspected faults, but the recognition of an accretionary origin resulted from the observation of pronounced discontinuities in lithology and paleobiology, combined with striking contrasts in paleomagnetism across the fault boundaries.

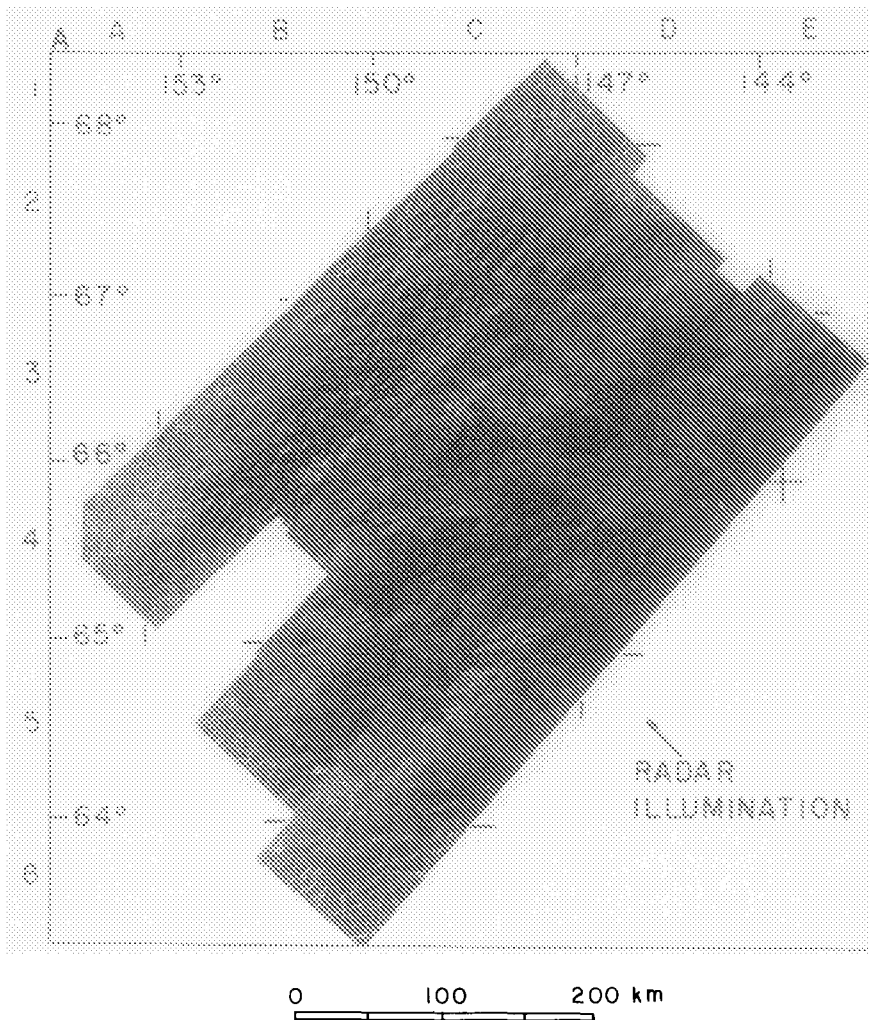


FIG. 8. Venera (A) and Magellan (B) radar image simulations of eastern interior, Alaska. The images are mosaics of 32 separate frames.

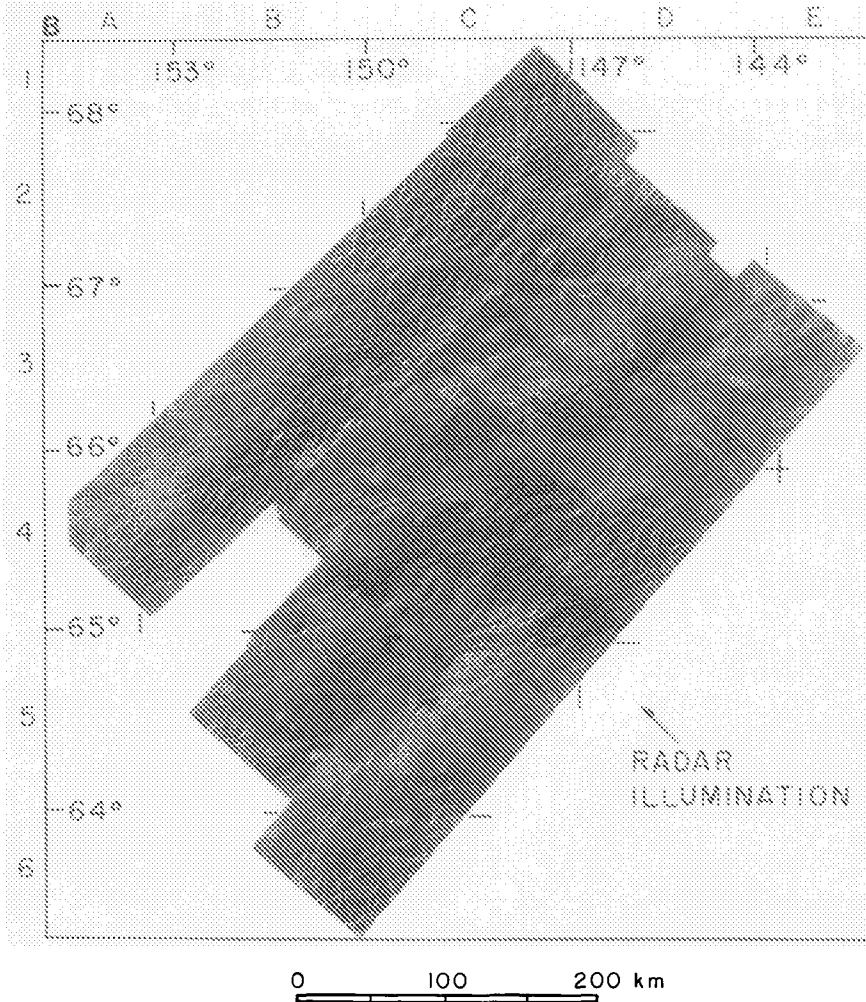


FIG. 8—Continued.

The distribution of accretionary terranes is not clear on either of the mosaics (Fig. 8). Specifically, the accretionary terranes are difficult to identify on images because (1) different terranes that have grossly similar lithologies appear to be texturally similar (cf. Angayucham and Tozitna terranes), (2) the traces of low-angle thrust faults that mark some terrane boundaries are commonly not distinguishable, (3) the fault traces that are distinguishable do not necessarily represent terrane boundaries, and (4) the distinction between lithotectonic ter-

ranes of accretionary origin and younger nonaccretionary plutons or sedimentary rock bodies of postaccretionary origin cannot be made from image data alone. In view of the above circumstances there would appear to be little possibility of correctly identifying lithotectonic accretionary terranes on images of the Venusian surface.

The Venera and the Magellan simulations both show a dominance of moderate to steeply sloping surfaces in the highland areas. The direction of radar illumination is toward the northwest across the mosaicked

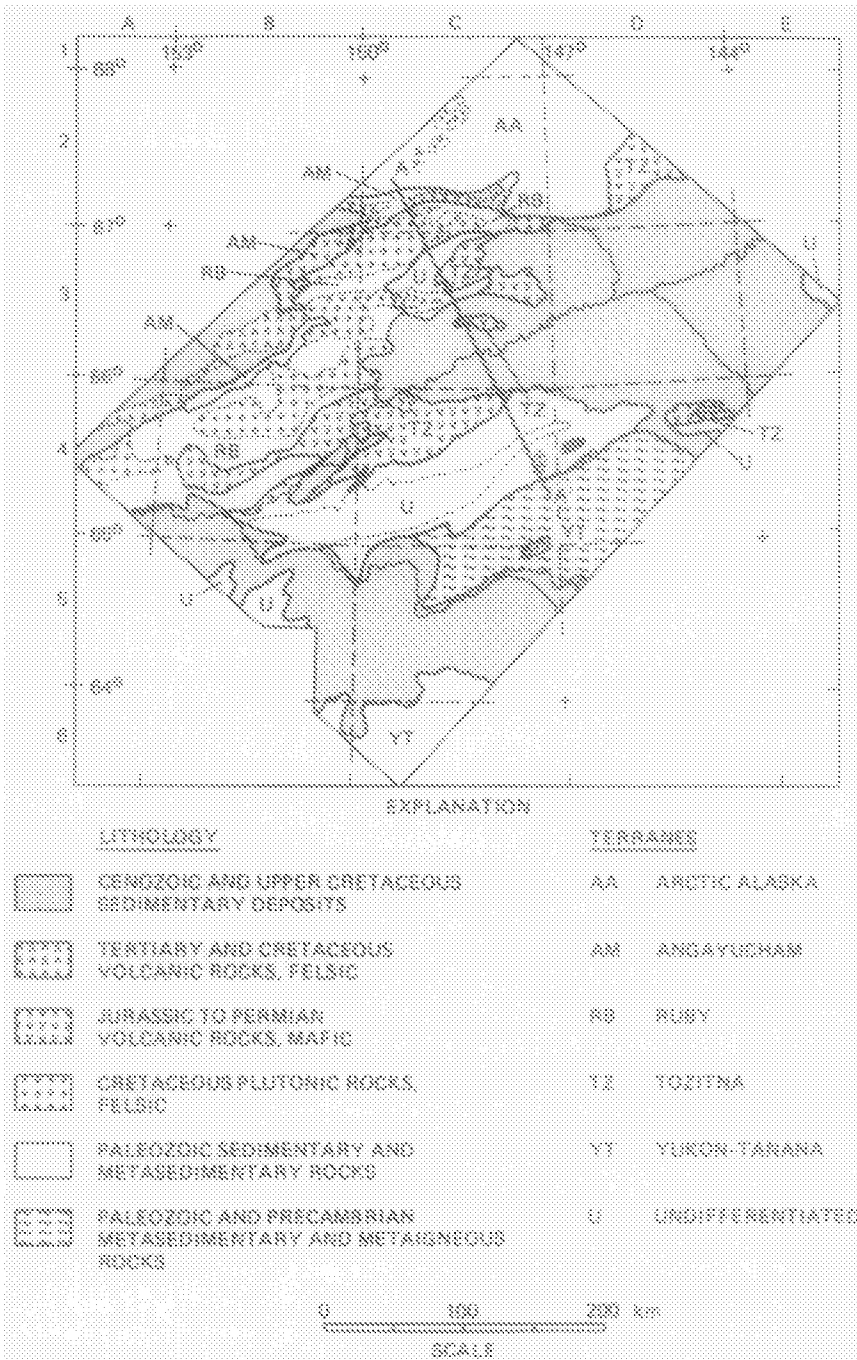


FIG. 9. Generalized lithology and distribution of lithotectonic terranes in area covered by Alaska simulations. Heavy lines denote terrane boundaries. Areas of complex or fragmentary terranes are not differentiated. Cross-section A-A' shown in Fig. 10.

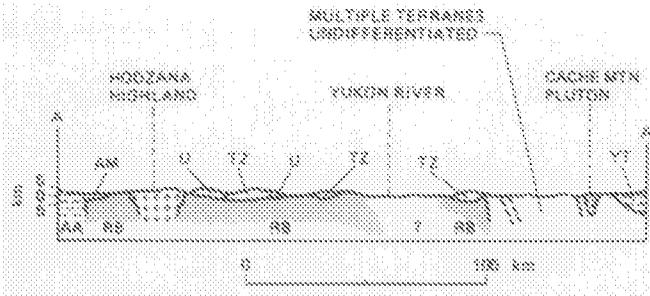


FIG. 10. Generalized cross-section A-A' extending south from Arctic Alaska terrane (AA) to Yukon-Tanana terrane (YT), showing Angayucham (AM) and Tozitna (TZ) terranes structurally above Ruby terrane (RB) (modified from Churkin *et al.* 1982, Jones *et al.* 1986).

image swaths. The radar sensitivity to slope distorts the topography in a strongly directional fashion and obscures most of the other surface characteristics in the highland areas. Even so it is possible to observe, on both simulations, broad tectonic fabrics that are imprinted on the highlands and dissection patterns that suggest significant modification by surficial processes. The Magellan simulation clearly portrays fluvial networks that demonstrate that water has been the dominant surficial agent.

Both simulations show that the mountains in the north have a blocky structure with dominantly east-trending facets and smooth valleys up to 10 km wide that widen southward in the direction of drainage. They follow linear and broadly arcuate traces with a symmetry that appears to be structurally controlled. The U-shaped form of the wide valleys seen in the Magellan simulation strongly suggests glacial erosion.

Marginal upland and contiguous lowland areas include the narrow but prominent Kobuk Trench, which separates the foothills of the Brooks Range from the Hodzana Highland (Fig. 8, lower margin of B-2 to D-2), the Yukon Flats District (B-3 to B-4 to E-3 to E-4), the Koyukuk-Kanutu Flats (B-3), and the Tanana-Kantishna Lowland (B-4 to B-5 to C-5). Level to gently undulating surfaces are common in the marginal upland and lowland areas, which range between about 100 and 330 m in elevation.

The regional drainage is WSW via the Yukon River. A few upper tributaries expose relatively wide channels of silt, sand, and gravel. Surficial deposits in the marginal upland and lowland areas consist largely of flood-plain alluvium and associated swamp and muskeg, glacial drift, eolian sand, and loess of late Cenozoic and Holocene age. In the marginal upland the deposits underlie dissected surfaces or they form alluvial fans and high-level terraces. In the adjacent lowlands the landforms include floodplains, low-level terraces, alluvial fans, sand dunes, and wide glaciated valleys (Williams 1962, Pewe *et al.* 1966, Patton 1973).

The Magellan mosaic (Fig. 8B) allows mapping of a number of features within the marginal uplands and lowlands. One of us (R.S.S.) constructed a detailed interpretation map from the Magellan data without prior knowledge of the area. Correct recognition of evidence for fluvial, periglacial, glacial, and aeolian processes reinforces our conclusion that the Magellan resolution allows rather detailed characterization of surficial processes. For example, in the Magellan simulation incised dendritic drainage can be seen traversing the radar-smooth surface of the marginal upland south and west of the Yukon River (C-3 to C-4 to D-3 to D-4, E-3). This type of drainage is characteristic of dissection in areas of homogeneous, friable deposits. The dissection also indicates a greater age for the deposits than for adjacent alluvium

in the floodplains. Mapping by Williams (1962) shows in fact that loess deposits are present in these areas. The deposits are not found north of the Yukon River, which suggests a northerly source area for the aeolian sediment.

Subtle linear patterns can be seen in enlargements of the Magellan simulation in the Kantishna and Tanana lowlands south of the Tanana River (B-5, C-5 upper left). The linear features are oriented northeast, approximately normal to the illumination direction of the radar, and are interpreted as stabilized aeolian dunes. Previous mapping has shown that the dunes are mostly longitudinal, up to 30 m high, 300 m wide, and 5 km long (Collins 1985).

On the Venera mosaic (Fig. 8A) the outline of the combined marginal upland and adjacent lowland areas is perceptible, and the pattern of regional drainage can be inferred. Because of the comparatively low spatial resolution of the image, however, the tones and patterns are diffuse. Consequently, subdued landforms are not distinguishable, and possible contrasts in the nature of the surface cannot be interpreted.

4. DISCUSSION

The Venera simulations discussed in the last sections demonstrate that many fine-scale surface textures due to weathering, erosion, and deposition are not discernable in radar images of terrestrial terrains. For example, the intricate drainage networks in the Appalachian and Alaska scenes are not discernable, nor are the dune complexes in the Gran Desierto. Although the topography associated with the Valley and Ridge Province is a consequence of differential erosion, and the etched patterns in the mountains in the Venera simulation of Alaska suggest degradation of tectonic landforms, the fine-scale textures present only in Magellan simulations provide the key observations needed to decipher the processes involved, i.e., fluvial, glacial, and aeolian.

The simulations also serve to remind us

that differential weathering and erosion are the rules rather than the exception on Earth. In fact, the excellent exposures of structural features on Earth are a direct consequence of variable rates of denudation of continental materials. Although denudation rates of the Earth's continents average about $10^2 \mu\text{m}/\text{year}$, there are variations of orders of magnitude from place to place, depending on local material properties, topography, and climate (Ritter 1978). Differential weathering and erosion also operate on Mars. For example, in comparing the degree of preservation of the volcanic rocks in Chryse Planitia with the debris deposits in Utopia Planitia, Arvidson *et al.* (1979) conclude that the rate of breakdown and removal of rock has been a small fraction of a micrometer per year. The rate of erosion of friable debris (in Utopia), on the other hand, has averaged about $1 \mu\text{m}/\text{year}$, consistent with Viking Lander observations of dust transport rates (Arvidson *et al.* 1983). The enhanced, albeit complicated, morphology of the higher Martian northern latitudes is probably a reflection of strong differential weathering and erosion. Ivanov *et al.* (1986) derive a resurfacing rate for Venus of 4×10^{-2} to $8 \times 10^{-1} \mu\text{m}/\text{year}$, based on the degree of preservation of radar-rough ejecta haloes around craters, together with an assumed cratering rate. If the upper bound is used, which may be more likely based on cratering rate and age analyses by Schaber *et al.* (1987), then over a billion years the equivalent of a kilometer high column of surface material would have been involved in resurfacing. For example, a kilometer of debris may have accumulated or a kilometer of material may have been eroded. Also, this estimate may be biased toward low values, since ejecta haloes seem to be preferentially located on plains. As on Mars, such deposits may withstand erosion by exposing hard, dense rock (e.g., Viking Lander 1 site).

Figure 11 shows a portion of quadrangle B-4, a mosaic of Venera image strips cen-

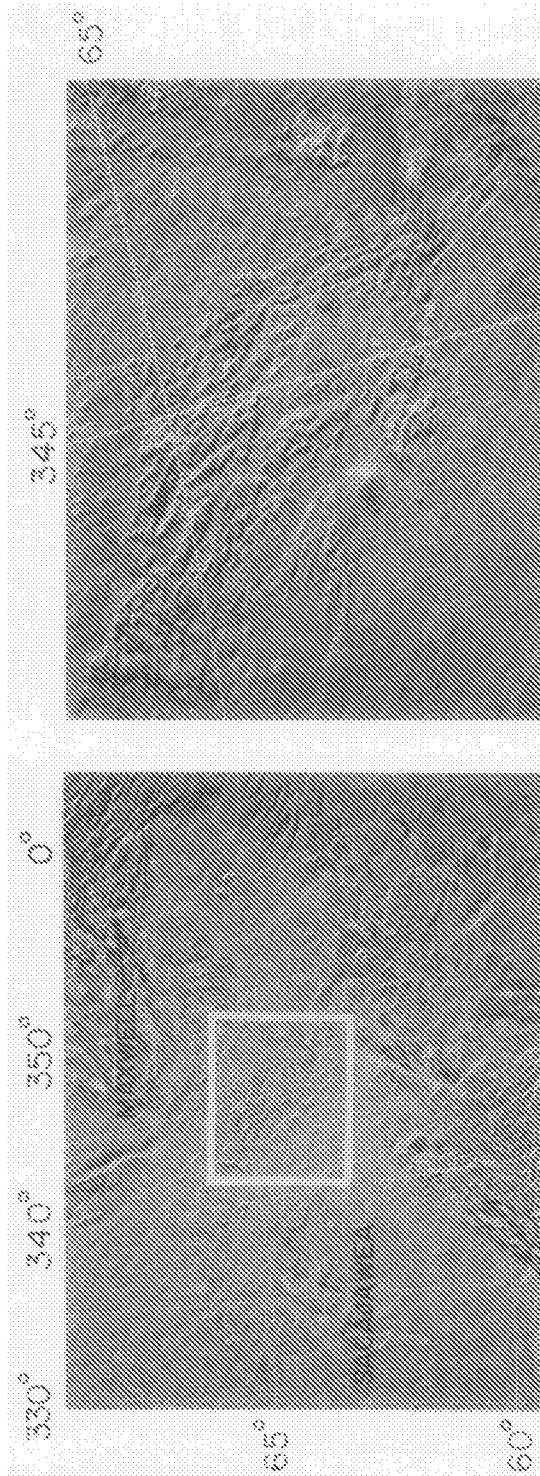


FIG. 11. Venera mosaic of portion of quadrangle B-4 shown on left, centered on eastern Lakshmi Planum. White box delineates area shown in enlarged form on right. Enlargement shows grooved terrain (terminology from Barsukov *et al.* (1986)) that has probably been embayed by highland plains. The grooved terrain has wide valleys and variegated ridges reminiscent of weathered and eroded terrains on Earth. The enlargement covers approximately the same area as the Alaska simulation shown in Fig. 8. Radar illumination direction is approximately from the left.

tered on eastern Lakshmi Planum. An enlargement of the eastern section of Lakshmi Planum is also shown in the figure. The Venera data were acquired with a steep look angle, corresponding to approximately a 10° incidence angle on a flat surface. At such a small angle, variations in slopes with length scales many multiples of the radar wavelength will control the backscatter signal strength. Thus, topographic information is primarily portrayed in the data. The enlargement shows a highly fractured terrain embayed by smooth plains materials. This landform has been called grooved terrain by Barsukov *et al.* (1986). The grooved terrain has wide linear valleys with rounded ridges and generally shows an etched or variegated appearance, including fine texture on ridge crests that is close to the resolution limit of the data. The appearance is reminiscent of the etched terrain seen in the Alaskan scene at Venera resolution. Venusian weathering and erosion may have widened valleys along fractures, and intervening ridges may have been rounded to form the grooved terrain.

Venera (and Earth-based) images of Venus clearly demonstrate that endogenic processes (volcanism, tectonism) have been active in shaping the surface (e.g., Barsukov *et al.* 1986). It is possible that the rates of volcanism and tectonism are so much higher than rates of atmospheric-related weathering, erosion, and transport that the resurfacing of Venus has been dominated in most areas by burial by volcanic materials and disruption by tectonism. On the other hand, we believe that it is also possible that the rates of atmospheric-related weathering and erosion have been high enough and have varied sufficiently with location (i.e., material properties of exposed units, altitude, etc.) to have caused significant differential weathering and erosion. For example, if divergent, convergent, and transform plate boundaries exist on Venus, sections of folded and faulted crust may have occasionally been exposed, including pieces of the upper

mantle. The exposed material may have weathered and eroded differentially, enhancing exposure of structures in ways analogous to processes operating on Earth, or analogous to the way the features in the higher northern latitudes of Mars have been enhanced by aeolian deflation. The grooved terrain shown in Fig. 11 would then be an older and/or more friable surface that has been subjected to enough weathering and erosion to display an etched appearance even at Venera resolution.

In summary, we believe that the existing collection of data for the venusian surface permits a wide range of resurfacing models. Magellan data, with an order of magnitude greater resolution than Venera data, should provide information on the key fine-scale textures (dunes, wind streaks, yardangs, deflation pits, exposed sedimentary layers, fine-scale etching, talus cones, perhaps even fluvial networks in oldest terrains, etc.) needed to refine and evaluate the extent to which the Venusian surface has been shaped by both endogenic and exogenic processes.

5. SUMMARY

(A) One-look Seasat radar images covering the Gran Desierto dune complex, Sonora, Mexico; the Appalachian Valley and Ridge Province; and accreted terranes in the central interior of Alaska were digitally processed to simulate both Venera 15, 16 images (1 to 3 km spatial resolution) of Venus and image data (120 to 300 m resolution) expected from the upcoming Magellan mission. Sinc filters were used to simulate the appropriate range and azimuth resolutions, speckle was introduced as multiplicative noise, and additive Gaussian noise was included to simulate expected signal to thermal noise ratios. The Sonora and Appalachian images each cover about 100×100 km. The Alaska scene is a digital mosaic of 32 Seasat frames and covers about 330×400 km.

(B) The Gran Desierto dunes, the largest complex in North America, are not dis-

cernable in the Venera simulation, whereas the higher resolution Magellan simulation shows the dominant dune patterns and specular reflections from dune faces oriented perpendicular to the incident radar. Anticlinal and synclinal structures are evident in both simulations over the Appalachians, mainly because differential weathering and erosion left resistant units (quartzites, sandstones, and conglomerates) as topographic highs that delineate the folds. The Magellan simulation also shows that fluvial processes have dominated erosion and exposure of the folded structures. Mountainous terrains and their degree of erosion are discernable in both simulations over Alaska, although only the Magellan simulation shows that fluvial, glacial, and aeolian processes have all been active in shaping the landscape.

(C) Neither simulation provides evidence that the Alaskan lithotectonic terranes were juxtaposed (i.e., accreted) by plate tectonic processes, since the primary evidence needed is lithological, whereas radar returns are dominated by topography and surface roughness, parameters only weakly indicative of lithology.

(D) The simulations show that morphologies that are diagnostic of terrestrial exogenic processes (fluvial, glacial, aeolian) have length scales that are typically too small to be discernable in images with Venera resolution. On the other hand, many diagnostic features are discernable in Magellan simulations, since the spatial resolution is an order of magnitude better than Venera resolution. Analyses by a number of researchers convincingly demonstrate that the surface of Venus is dominated by volcanic and tectonic landforms. However, the simulations suggest that given the resolution of current data, it would be difficult to tell whether or not a significant amount of atmosphere-surface weathering, erosion, and deposition has also occurred. For example, differential weathering and erosion may have significantly modified both volcanic and tectonic features. Magellan

data should provide information on key fine-scale features (dunes, yardangs, fine-scale etching, etc.) needed to evaluate the importance of both endogenic and exogenic processes in modifying the Venusian surface.

ACKNOWLEDGMENTS

This work was funded in part by NASA Grant NSG-7087 to Washington University by the NASA Planetary Geology and Geophysics Program and by NASA support to the Jet Propulsion Laboratory. Thanks are due to James W. Head III for access to the Venera image data and for reviewing the manuscript. Comments from Gordon Pettengill are also appreciated. Special thanks to our Soviet colleagues for allowing U.S. investigators access to Venera data. Access was facilitated by the Brown University-Vernadsky Institute agreement.

REFERENCES

- ARVIDSON, R. E., E. A. GUINNESS, AND S. LEE 1979. Differential aeolian redistribution rates on Mars. *Nature* **278**, 533-535.
- ARVIDSON, R. E., E. A. GUINNESS, H. J. MOORE, J. TILLMAN, AND S. D. WALL 1983. Three Mars Years: Mutch Memorial Stations (Viking Lander 1) imaging observations. *Science* **222**, 463-468.
- BARSUKOV, V. L., A. T. BASILEVSKY, G. A. BURBA, N. N. BOBINA, V. P. KRYUCHKOV, R. O. KUZMIN, O. V. NIKOLAEVA, A. A. PRONIN, L. B. RONCA, I. M. CHERNAYA, V. P. SASHKINA, A. V. GARANIN, E. R. KUSHKY, M. S. MARKOV, A. L. SUKHANOV, V. A. KOTELNIKOV, O. N. RZHIGA, G. M. PETROV, YU. N. ALEXANDROV, A. I. SIDORENKO, A. F. BOGOMOLOV, G. I. SKRYPNIK, M. YU. BERGMAN, L. V. KUDRIN, I. M. BOKSHEIN, M. A. KRONROD, P. A. CHOCHIA, YU. S. TYUFLIN, S. A. KADNICHANSKY, AND E. L. AKIM 1986. The geology and geomorphology of the Venus surface as revealed by the radar images obtained by Veneras 15 and 16. *Proc. Lunar Planet. Sci. Conf. XVII, Part 2, J. Geophys. Res.* **91**, D378-D398.
- BASILEVSKY, A. T., A. A. PRONIN, L. B. RONCA, V. P. KRYUCHKOV, AND A. L. SUKHANOV 1986. Styles of tectonic deformations of Venus: Analysis of Venera 15 and 16 data. *J. Geophys. Res.* **91**, D399-D411.
- BEIKMAN, H. M. (compiler) 1980. *Geologic Map of Alaska: U.S. Geological Survey*. Washington, DC, scale 1:2,500,000.
- BINDSCHADLER, D. L., AND J. W. HEAD 1988. Characterization of Venera 15/16 geologic units from Pioneer-Venus reflectivity and roughness data. *Icarus*, in press.
- BLOM, R., AND C. ELACHI 1981. Spaceborne and

- airborne imaging radar observations of sand dunes. *J. Geophys. Res.* **86**, 3061–3073.
- CAMPBELL, D. B., J. W. HEAD, J. H. HARMON, AND A. A. HINE 1983. Venus: Identification of banded terrain in the mountains of Ishtar Terra. *Science* **221**, 664–647.
- CAMPBELL, D. B., J. W. HEAD, J. H. HARMON, AND A. A. HINE 1984. Venus: Volcanism and rift formation in Beta Regio. *Science* **226**, 167–170.
- CHURKIN, M., JR., H. L. FOSTER, R. M. CHAPMAN, AND F. R. WEBER 1982. Terranes and suture zones in east central Alaska. *J. Geophys. Res.* **87**, 3718–3730.
- COLLINS, F. R. 1985. *Map Showing a Vegetated Dune Field in Central Alaska*. U.S. Geological Survey, Misc. Field Studies, Map MF-1708 with text, scale 1:250,000.
- CONEY, P. J., D. L. JONES, AND J. W. H. MONGER 1980. Cordilleran suspect terranes. *Nature* **288**, 329–333.
- CRUMPLER, L. S., J. W. HEAD, AND D. B. CAMPBELL 1986. Orogenic belts on Venus. *Geology* **14**, 1031–1034.
- CURLANDER, J. C., R. KWOK, AND S. S. PANG 1987. A post-processing system for the rectification and registration of spaceborne SAR imagery. *Int. J. Remote Sen.* **8**, 621–638.
- GOLDFINGER, A. D. 1982. Estimation of spectra from speckled images. *IEEE Trans. Aerosp. Electron. Syst.* **AES-18**.
- GREELEY, R., P. R. CHRISTENSEN, J. F. MCHONE, Y. ASMEROM, AND J. R. ZIMBELMAN 1985. *Analysis of the Gran Desierto–Pinacate Region, Sonora, Mexico, via Shuttle Imaging Radar*. NASA Contractor's Report 177356.
- IVANOV, B. A., A. T. BASILEVSKY, V. P. KRYUCHKOV, AND I. M. CHERNAYA 1986. Impact craters of Venus: Analysis of Venera 15 and 16 data. *J. Geophys. Res.* **91**, D413–D430.
- JONES, D. L., N. J. SILBERLING, H. C. BERG, AND G. PFLAKER 1981. *Map Showing Tectonostratigraphic Terranes of Alaska, Columnar Sections, and Summary Description of Terranes*. U.S. Geological Survey, Open-File Report 81-792, map and text, scale 1:2,500,000.
- JONES, D. L., N. J. SILBERLING, AND P. J. CONEY 1986. Collision tectonics in the cordillera of western North America: Examples from Alaska. In *Collision Tectonics* (M. P. Coward and A. C. Ries, Eds.), pp. 367–387. Geological Society Special Publication No. 19, London.
- JONES, D. L., N. J. SILBERLING, P. J. CONEY, AND G. PFLAKER 1984. Lithotectonic terrane map of *Lithotectonic Terrane Maps of the North American Cordillera* (N. J. Silberling and D. L. Jones, Eds.). U.S. Geological Survey, Open-File Report 84-523. Maps and text, scale 1:2,500,000.
- JURGENS, R. F., R. M. GOLDSTEIN, H. R. RUMSEY, AND R. R. GREEN 1980. Images of Venus by three station interferometry—1977 results. *J. Geophys. Res.* **85**, 8282–8294.
- KWOK, R., J. C. CURLANDER, AND S. S. PANG 1987. Rectification of terrain-induced distortions in radar imagery. *Photogramm. Eng. Remote Sens.* **5**, 507–513.
- KWOK, R., J. C. CURLANDER, AND S. S. PANG. Unsupervised digital mosaic of spaceborne SAR imagery, in preparation.
- PATTON, W. W., JR. 1973. *Reconnaissance Geology of the Northern Yukon–Koyukuk Province, Alaska*. U.S. Geological Survey, Prof. Paper 774-A.
- Pennsylvania Geological Survey, *Geologic Map of Pennsylvania 1960*. Washington, DC. Commonwealth of Pennsylvania, Pennsylvania Geological Survey, Topographic and Geologic Survey and U.S. Geological Survey, scale 1:250,000.
- PEWE, T. L., C. WAHRHAFTIG, AND F. WEBER 1966. *Geologic Map of the Fairbanks Quadrangle, Alaska*. U.S. Geological Survey Misc. Geological Investigations, Map I-545 with text, scale 1:250,000.
- RITTER, D. F. 1978. *Process Geomorphology*, 2nd ed. W. C. Brown, Dubuque, IA.
- RODGERS, J. 1982. The life history of a mountain range—The Appalachians. In *Mountain Building Processes* (K. J. Hsu, Ed.), Chaps. 2–8, pp. 229–242. Academic Press, New York.
- SCHABER, G. G., E. M. SCHOEMAKER, AND R. C. KOZAK 1987. Is the Venusian surface really old? *Lunar and Planetary Science Conference XVIII*, 874–875.
- WILLIAMS, J. R. 1962. *Geologic Reconnaissance of the Yukon Flats District, Alaska*. U.S. Geological Survey, Bull. 1111-H, 289-331 with map, scale 1:500,000.